water

MDPI

Article

An Integrated Approach Based on Numerical Modelling and Geophysical Survey to Map Groundwater Salinity in Fractured Coastal Aquifers

Costantino Masciopinto *, Isabella Serena Liso, Maria Clementina Caputo and Lorenzo De Carlo

National Research Council, Water Research Institute, via Francesco De Blasio 5, 70132 Bari, Italy; serena.liso@ba.irsa.cnr.it (I.S.L.); maria.caputo@ba.irsa.cnr.it (M.C.C.); lorenzo.decarlo@ba.irsa.cnr.it (L.D.C.)
* Correspondence: costantino.masciopinto@ba.irsa.cnr.it; Tel.: +39-080-5820-537

Received: 27 July 2017; Accepted: 7 November 2017; Published: 10 November 2017

Abstract: Aquifer over-exploitation may increase coastal seawater intrusion by reducing freshwater availability. Fractured subsurface formations commonly host important freshwater reservoirs along sea coasts. These water resources are particularly vulnerable to the contamination due to seawater infiltration occurring through rapid pathways via fractures. Modeling of density driven fluid flow in fractured aquifers is complex, as their hydrodynamics are controlled by interactions between preferential flow pathways, 3D interconnected fractures and rock-matrix porosity distribution. Moreover, physical heterogeneities produce highly localized water infiltrations that make the modeling of saltwater transport in such aquifers very challenging. The new approach described in this work provides a reliable hydrogeological model suitable to reproduce local advancements of the freshwater/saltwater wedge in coastal aquifers. The proposed model use flow simulation results to estimate water salinities in groundwater at a specific depth (1 m) below water table by means of positions of the Ghyben-Herzberg saltwater/freshwater sharp interface along the coast. Measurements of salinity in 25 boreholes (i.e., salinity profiles) have been used for the model calibration. The results provide the groundwater salinity map in freshwater/saltwater transition coastal zones of the Bari (Southern Italy) fractured aquifer. Non-invasive geophysical measurements in groundwater, particularly into vertical 2D vertical cross-sections, were carried out by using the electrical resistivity tomography (ERT) in order to validate the model results. The presented integrated approach is very easy to apply and gives very realistic salinity maps in heterogeneous aquifers, without simulating density driven water flow in fractures.

Keywords: fractured aquifers; seawater intrusion; flow modeling; salinity map; groundwater ERT

1. Introduction

Seawater encroachments may lead to a consistent reduction of freshwater volume availability. Mathematical models are very useful to simulate seawater intrusion in coastal aquifers, as for instance in order to locate the freshwater/saltwater sharp interface position along coastal areas. There are specific numerical codes produced by academic institutions, such as the United States Geological Survey (USGS, Reston, VA, USA) or by commercial software houses, such as Aquanty, Inc. (Waterloo, ON, Canada), that can provide largely utilized models such as FEFLOW [1], SUTRA [2], SEAWAT-2000 [3] or HydroGeoSphere [4]. These are specific codes to study transient density driven flow of seawater inland advancements in coastal aquifers, even by 3D visualization. Anyway, the application of these codes in a fractured aquifer may have severe limitations when heterogeneities and the preferential water flow pathways in fractures are not properly taken into account in the governing equations.

This is because the representative elementary volume (REV) of the fractured groundwater, to which we must refer all model parameters (i.e., constant hydraulic conductivity and transmissivity, porosity, storativity, etc.) and variables of the flow and transport equations, it may have a very large size which renders unsuitable the application of the conventional models above mentioned. Moreover, the REV of a fractured aquifer might not exist when the constancy of parameters is not achieved in the entire size of the computational domain.

The only method to overpass this obstacle is to apply the governing flow and transport equation to a REV of the flowing fluid in each single fracture. This can be possible when the geometry of the fluid flow pathway is known a priori. Thus, specific methods are required to reproduce and address into the model all preferential flow geometries that occur in different fractures of the coastal studied aquifer. Different conceptual model can be defined in fractured media, even by taking into account of tortuosity of the flow pathways [5]. Major stochastic media idealization for modeling the flow in fractured rocks lead to: the fracture zone continuum model [6], where the fractured aquifer is considered as an equivalent heterogeneous porous medium and the "discrete" fracture networks [7–9]. Most used in coastal areas is the flow in a set of parallel and identical fractures (i.e., layered model) [10]. In this work, the stochastic method reproduced into the model, the geometry of real preferential water flow pathways of the Bari fractured aquifer. The selected stochastic method was able to transfer all real medium heterogeneities into the computation procedure. Valid stochastic methods can provide appropriate numeric model solutions not only in fractured aquifers, but also in a generic heterogeneous aquifer. The stochastic method applied in this work investigated the spatial variability of the sizes of fracture apertures of the Bari groundwater.

Groundwater flow at the regional scale (>1000 m), is usually mediated into the vertical thickness (z) by considering a prevalent mean horizontal flow (x, y), as the saturated (vertical, z) thickness is usually less than 50 m [11]. In the present work, instead, the groundwater flow modeling was addressed in a 3D set made by N_f parallel fractures, which have the same mean aperture value $2b_m$ and an impermeable rock matrix. To support the stochastic method in this work, the data derived from pumping tests on wells were necessary to implement the real heterogeneities of the filtration medium into each single fracture of the model.

The flow simulation results defined the freshwater/saltwater (50%) sharp interface position in the Bari aquifer by using the Ghyben-Herzberg theory and highlighted the part of the costal aquifer where the seawater encroachment was present. In order to validate the spatial distribution of water salinity close to seawater encroachment in groundwater, the numerical results were compared with geo-electrical measurements carried out in two separated groundwater zones. These field investigations utilize non-invasive geophysical techniques for monitoring coastal aquifer salinity dynamics. The geophysical survey, particularly, the electrical resistivity tomography (ERT), is a powerful tool to evaluate the heterogeneity of subsoil by estimating groundwater salinity at specific depths below the ground. The ERT can be very useful when few boreholes (i.e., data) are available for direct measurements by probes of groundwater salinity. Furthermore, monitored salinity profiles in boreholes are affected by water salt mixing into the water columns and by vertical saltwater stratification due to density. Thus, the real water salinity in a fracture at a specific depth can be accurate only by installing packers into the well. These devices can isolate specific water depth intervals into the borehole by providing appropriate salinity concentrations with depth. However the packers are not easy to apply because they cannot be applied in boreholes with large diameter. Moreover packer installation can be efficiently made only in unscreened wells. Subsequently, errors on direct measurements of water salinity in boreholes might increase the uncertainty of model predictions.

In the literature there are many papers [12–21] concerning the application of the ERT technique to detect the fresh/saltwater sharp interface in groundwater by visualizing the inland zone of saltwater encroachment. Usually ERT is applied to obtain a qualitative result, which is a function of the electrical resistivity contrast between the freshwater and the saltwater contained in the investigated groundwater volume. However, quantitative estimations of water salinity concentrations by using resistivity

measurements have been provided by Wagner et al. [22] and Singha et al. [23]. These researchers defined a specific petro-physical relationship based on the Archie's law [24] in order to derive water salinities.

In present study a new site specific relationship resistivity/salinity has been defined in order to infer salinity data by ERT survey in two coastal sections (y, z) of the Bari groundwater. These salinity data have been then successful compared with results (i.e., salinity map) given by model at the depth of 1 m below water table. The good agreement of the trends of ground water salinity suggests that ERT is a powerful tool to provide suitable data of groundwater salinity in coastal areas by supporting flow and salt transport model validations.

2. Materials and Methods

The field tests, carried out at the Bari site (Figure 1), have been conducted at the top of a karstic fractured limestone formation that hosts the Murgia aquifer. The water table ranges from 5 to 40 m below the ground.

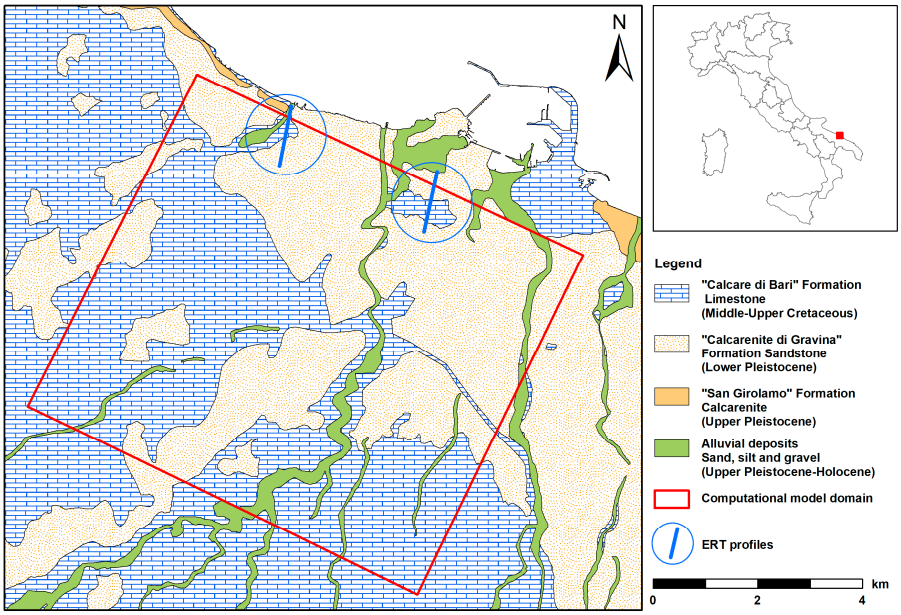

Figure 1. Bari site geological sketch and computational domain (red square) for groundwater flow and Ghyben-Herzberg simulations, and the positions of the electrical resistivity tomography (ERT) profiles of subsoil.

A detailed geological description of the Bari coastal aquifer is available in [25]. The study area lies on the eastern edge of the Murge, that represents the central part of the foreland of the Southern Apennine mountains [26], characterized by a thick Mesozoic sedimentary sequence, overlain by relatively thin and discontinuous Quaternary deposits. Locally, the "Calcare di Bari" represents the outcropped Mesozoic sequence formation (Figure 1) characterized by numerous karstic cavities of different shapes and sizes, partially or completely filled by "terra rossa" deposits. "Calcarenite of Gravina" (Lower Pleistocene) represents the Quaternary formation, consisting of litho-bioclastic sandstone. Colluvial and eluvial deposits (Upper Pleistocene-Holocene) cover stream beds (i.e., Lame), while narrow bands, as outcrops of well-cemented porous sandstone (Upper Pleistocene) appear along the coast. Limestone bedrock hosts a wide and thick aquifer. High limestone permeability is the result of the intense fracturing of rock and of the karst dissolving action. The irregular spatial distribution of the fractures and karstic channels renders the Bari aquifer very anisotropic. The groundwater flows toward the sea, under a low pressure, in different subparallel fractured layers separated

by compact (i.e., not fractured) blocks of rock. In particular, along a generic water flow pathway, the fracture apertures with small sizes control the gradient line of predominant horizontal freshwater flow, i.e., small sized apertures are the bottlenecks of the freshwater flow. In the study area, hydraulic transmissivity, T [L^2/t], and conductivity, K [L/t], of the "Calcare di Bari" formation, have been determined by inverting the steady radial flow solution to a well (i.e., the Thiem's equation) [27]. Results given by thirty-six (Table 1) pumping-well tests provide the experimental variogram of fracture apertures of the coastal aquifer. The model estimated the local fracture apertures by inverting mean aquifer conductivity formula, i.e., $K = \gamma_w/\mu \times nb^2/3$, where n [-] is the effective porosity of the saturated freshwater thickness. In fact the hydraulic conductivity in a single (smoothed) fracture with aperture $2b$, was obtained by comparing the velocity defined by Hagen-Poiseuille equation, which is usually adopted [28] to determine the plane flow velocity in a fracture, with the velocity provided by Darcy equation.

Table 1. Estimations of the mean fracture apertures at the Bari coastal aquifer, by inverting the solution of the steady radial water flow to a well during pumping.

X (m)	*Y* (m)	*K* (m/s)	Well ID	2*b* (mm)
		Pumping Test		
654,627.88	4,548,060.78	4.05×10^{-6}	PT1	248.79
654,668.04	4,548,542.57	2.40×10^{-5}	PT2	336.14
655,009.30	4,548,492.39	2.21×10^{-5}	PT3	331.71
654,979.19	4,548,151.12	4.90×10^{-5}	PT4	378.25
656,378.54	4,549,873.53	6.64×10^{-4}	PT7	629.59
648,038.69	4,552,384.46	1.86×10^{-5}	PT8	322.25
648,794.68	4,551,906.47	1.14×10^{-5}	PT9	297.27
648,351.69	4,551,897.47	2.32×10^{-5}	PT10	334.38
647,309.71	4,551,475.47	2.76×10^{-5}	PT11	344.01
647,914.70	4,551,580.47	1.92×10^{-5}	PT12	324.11
648,341.69	4,551,249.48	5.77×10^{-5}	PT13	388.76
648,686.68	4,551,472.47	2.66×10^{-5}	PT14	342.00
653,466.00	4,552,424.00	2.71×10^{-3}	IS1	958.84
655,868.00	4,554,156.00	4.25×10^{-4}	IS2	566.99
655,515.00	4,552,586.00	9.74×10^{-5}	IS4	425.37
655,272.00	4,552,018.00	6.40×10^{-6}	IS5	269.43
654,726.00	4,551,838.00	1.19×10^{-5}	IS7	299.38
654,599.00	4,551,852.00	7.25×10^{-5}	IS8	404.13
651,985.00	4,553,569.00	3.80×10^{-3}	IS9	1089.42
651,172.00	4,552,620.00	9.25×10^{-6}	IS10	286.87
651,558.00	4,550,230.00	2.37×10^{-4}	IS11	501.40
650,678.00	4,554,592.00	3.45×10^{-5}	IS13	356.91
651,256.00	4,554,586.00	1.47×10^{-5}	IS14	310.07
647,153.00	4,553,736.00	6.26×10^{-6}	IS19	268.41
645,754.00	4,553,926.00	7.03×10^{-6}	IS21	273.81
653,419.00	4,549,497.00	3.72×10^{-5}	IS22	361.33
654,415.00	4,550,306.00	1.27×10^{-5}	IS23	302.37
654,812.00	4,550,479.00	1.26×10^{-5}	IS24	302.08
654,559.00	4,551,970.00	1.19×10^{-5}	IS25	299.38
656,315.00	4,552,223.00	5.48×10^{-5}	IS26	385.45
656,919.00	4,550,832.00	1.47×10^{-5}	IS28	310.07
652,850.93	4,553,352.70	4.17×10^{-3}	L4	1130.53
653,252.50	4,555,151.70	2.17×10^{-3}	PSUD	887.25
652,430.90	4,554,429.80	6.43×10^{-3}	L3-S	1360.49
647,930.70	4,551,813.20	1.33×10^{-4}	L5-S	449.84
654,679.50	4,555,109.10	2.29×10^{-3}	L12-S	903.60
Mean value		6.58×10^{-4}		471.69

It should be noted that during the field investigation only 25 wells of 36 listed in Table 1 were accessible to carry out water depth and salinity measurements.

2.1. Fractures Description and Flow Solutions: Experimental Tests

The fracture aperture size at grid position (x, y) was generated by the following stationary random field, ε

$$\varepsilon(x,y) = Y(x,y) - \overline{Y} \tag{1}$$

where is $Y = \log 2b$ and $\overline{Y}$ is its mean. The semi-variogram model [5] of the expected value of the variance is:

$$\gamma(\xi_{xy}) = \frac{1}{2}E\left[\left\{\varepsilon(x,y) - \varepsilon\left(x+\xi_x, y+\xi_y\right)\right\}^2\right] \tag{2}$$

which can be derived using the autocovariance function

$$R(\xi_{xy}) = \sigma^2_{xy} \exp\left[\left(\frac{\xi_x^2}{\zeta_x^2} + \frac{\xi_y^2}{\zeta_y^2}\right)^{1/2}\right] \tag{3}$$

where the unknown semi-variogram model parameters ${\sigma^2}_{xy}$ (sill + nugget), ξ_x and ξ_y and (i.e., correlation lengths) can be calculated using SURFER (Golden Software Inc., Golden, CO, USA) on the basis of the spatial distribution of mean apertures determined from the results of pumping tests. For the Bari coastal aquifer, the best-fit of the experimental semi-variogram was made using the exponential model (Figure 2) with ${\sigma^2}_{xy} = 0.268$, $\xi_x = 1000$ m and $\xi_y = 2000$ m, using data derived from thirty-six tests (Table 1). However, at the field scale, it should also be considered the uncertainty (~15%) due to the prediction of the spatial covariance of fracture apertures, which is dependent upon the available number of field measurements (i.e., well pumping-tests). This uncertainty was due to non-ergodicity of the scholastic variable [29].

The flow rate in each channel in x direction with cross section $2b \times \Delta y$ (or $2b \times \Delta x$, in y direction) can be estimated by revising the Darcy-Welsbach equation ([28] p. 126).

$$\left(\phi_i - \phi_j\right) = {Q_{ij}}^2\left[\frac{f}{2g\Delta y}\frac{\Delta x}{\Delta y}\left(\frac{1}{(2b_i)^3} + \frac{1}{(2b_j)^3}\right)\right] \tag{4}$$

where the friction factor f [-] can be derived from the Reynolds number [22] even for non-laminar or turbulent fluxes; g is gravity acceleration and Q_{ij} [L^3/t] = $U \times 2b \times \Delta x \Delta y$, is the local discharge between grid nodes i and j into the single fracture, where Δx and Δy are the discretization grid steps. The finite difference method can be used to solve the continuity equation (i.e., $\Sigma Q = 0$) applied to each grid node of the discretized domain. The resulting set of equations was solved by the iterative successive-over-relaxation (SOR) method by using as boundary conditions the piezometric heads into the depressed areas (i.e., pumping wells) and along the border of the studied area.

Ghyben-Herzberg Freshwater/Saltwater Sharp Interface

The flow simulation results enabled the estimation of the 50% freshwater/saltwater interface positions with respect to the coastline by applying the Ghyben-Herzberg equation. Indeed, to predict the interface toe position L [L], with respect to the coastline, the resulting total groundwater freshwater outflow given by Equation (4) was managed to calculate the length of intrusion for every position along the coast [30]

$$L - L_d = K\frac{B^2 - H_s^2}{2\delta_\gamma \times Q_0} - L_d = n\frac{b_i^2}{3}\frac{\gamma_w}{\mu}\frac{\left(\delta_\gamma \times \phi_0\right)^2 - H_s^2}{2\delta_\gamma \times Q_0^i} - L_d \tag{5}$$

where L_d [L] is the distance of the contour head ϕ_0 (for instance of 1 m) from the coastline given by the flow simulation results; H_s [L] is the freshwater head at the outflow section (usually set to 0); $Q^i{}_0$ [$L^3/t/L$] is the groundwater (i.e., freshwater) discharge along the coast predicted by the model at grid node i; B [L] is the aquifer saturated thickness where is $\phi = \phi_0$; and $\delta_\gamma = \gamma_w/(\gamma_s - \gamma_w)$ is the ratio of the water specific weights.

In each single fracture of the Bari aquifer, the distance d of the generic grid node (x, y) from the sharp interface was converted into a salinity concentration by using the empirical formula [31]

$$C_{salt} = C_{s0} + A_s\left[\exp\left(-\frac{d}{D_s}\right)\right] \quad (6)$$

where the best fit constants C_{s0} = 1.54 g·L^{-1}, A_s = 12.02 g·L^{-1} and D_s = 592.65 m were estimated by fitting the groundwater salt concentrations measured in twenty-five boreholes of the coastal aquifer, at the depth of 1.0 m below the water table.

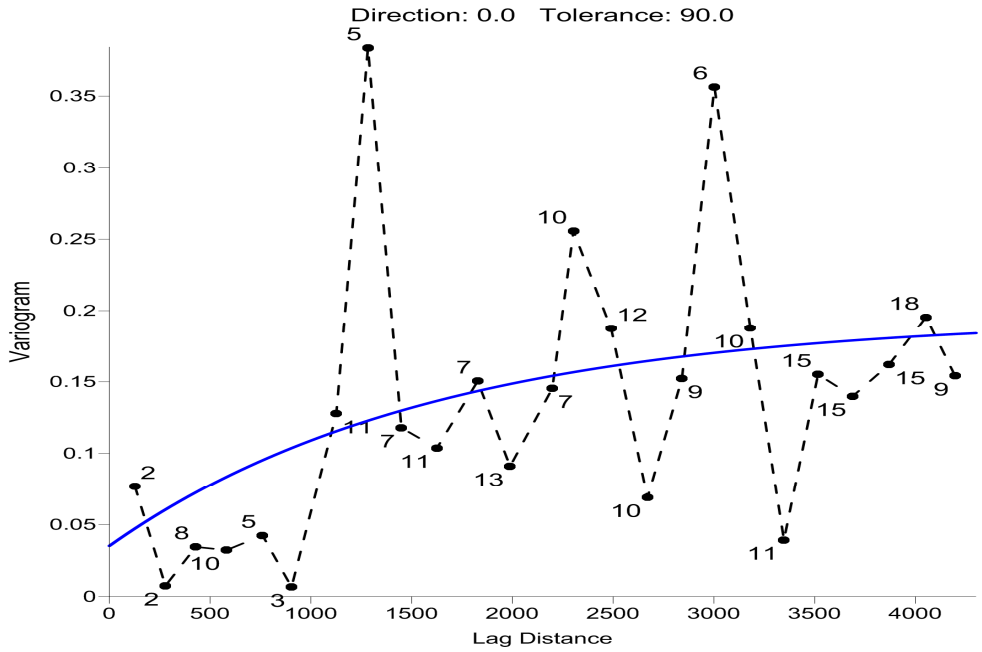

Figure 2. Experimental aperture variogram and model variogram parameters at Bari (Southern Italy) coastal fractured aquifer; Model: Exponential (Scale = 0.16; Length = 3000 m; Anisotropy: ratio = 2, angle = 64.5 degrees; Nugget Effect: error = 0.03518, micro = 0); Experimental: max lag distance = 4300 m, number of lag = 25, lag width = 172 m, vertical scale = 0.384.

2.2. ERT Survey

ERT is a non-invasive and cost-effective geophysical technique commonly used for spatial characterization of the subsoil over extended areas.

Soil electrical resistivity (i.e., the inverse of electrical conductivity) is an intrinsic parameter of the soil, which can quantify the resistance of a given porous medium to the flow of the electric current. Many factors affect the electrical resistivity of the medium, such as rock (or soil) porosity, clay content, and salinity and temperature of water. Among these, water content and water salinity are the most important parameters because the electric current flows into the rock by means of dissolved electrolyte ions (i.e., dissolved salts) of the water in the pore spaces of the soil or in fractures. In the field, electrical resistivity data are usually measured by using an array of four electrodes: two electrodes are used to insert the electric current into the ground, and other two electrodes are used to measure the difference of electrical potential into the investigated rock volume. The measurement, which is the apparent

resistivity of a homogeneous bulk volume of the soil (or the rock) to which the measured electrical resistance is equivalent [32], is then calculated by multiplying the resistance of the medium by a geometrical factor, which depends on the arrangement (i.e., geometry and distance) of the electrodes of the array. The subsequent inversion process, based on an iterative numerical method, allows us to minimize the misfit between the theoretical resistivity and the measured one. This last numerical method is usually required to estimate a more realistic resistivity distribution of the investigated soil.

In the study area, the ERT survey has been collected through a sequence of ten (y, z) ERT profiles, grouped into two main subsurface cross sections. Each section was about 1 km of length in the direction perpendicular to the coastline. These sections were located in two separated coastal areas. The first area (Line A) was positioned where model results highlighted the seawater encroachment in groundwater. The second section (Line B), instead, was located where the model simulation has shown a freshwater outflow into the sea. The first section (Line A) grouped five ERT profiles, from E1 to E5, whereas the section Line B, grouped other five ERT profiles, from E6 to E10 (Figure 3). ERT was carried out using the Syscal Switch Pro 48 (IRIS Instruments, Orleans, France) resistivity-meter. A Wenner–Schlumberger configuration array provided a good arrangement by considering the depth of investigation (<30 m) below the ground and lateral resolution (<3 m). The length of each ERT profile was changed according to the required depth of the investigation below the ground, which was dependent upon the expected groundwater depth. Therefore, E1, E6 and E7 profiles were 135–160 m of length, while remaining profiles were length about 50 m. For each ERT profile, 1500 data points were collected, including both direct and reciprocal measurements required for the data quality control. This is because following the reciprocity principle when the previous current electrodes are switched to the potential electrodes the same resistivity values should be expected. The operating parameters during the acquisitions (Table 2) were settled to optimize the field electrical resistivity measurements.

Figure 3. ERT profile locations. Blue points are boreholes (six) used for salinity measurements to calibrate Equation (7) by using resistivity data provided by ERT profiles.

Table 2. Transmission (i.e., operating) parameters used in ERT surveys.

Injection Pulse Duration	250 ms
Minimum and maximum number of cycles for each measurement	3–6
Standard deviation of the measurements in a cycle	5%

The parameter optimization allowed bad data points removal when threshold values (i.e., the noise) were overcome, as is shown in Table 3. The low number of removed data (5%) confirmed the good quality of the ERT sequence. The inversion was made by using code RES2DINV (Geotomosoft Solutions, Gelugor, Malaysia).

Table 3. Error bounds during ERT data filtering.

Parameter	Lower Bound	Upper Bound
Injection current (mA)	5	1000
Potential measurement (mV)	5	5000
Deviation standard of the measurements in a cycle (%)	0	5
Percentage difference between direct and reciprocal data (%)	0	5

Usually, in order to estimate groundwater salinity from resistivity collected data a relationship based on the Archie's law could be applied. In the proposed study, Archie's law, did not yield satisfactory results, due to the wide heterogeneity of the fractured aquifer investigated, which present preferential water flow pathways. In such complex hydrogeological formations, it might be challenging to calibrate the Archie's law due to variability of the rock quality, i.e., porosity, cementation index, etc., and of the water salinity in the bulk volume investigated by ERT.

For these reasons, a new site-specific relationship of the resistivity-salinity concentration (ρ-C_{salt}) was proposed. For this investigation, additional six ERT profiles were performed close to the boreholes where the salinity of groundwater at 1 m of depth was directly measured using an electrical conductivity probe (MS5 OTT, Inc., Kempten, Germany). This means that from the twenty-five boreholes we selected six at different water salinities to carry out six additional ERT. We selected only six ERT/wells for a technical reason (i.e., low groundwater depth <3 m). In fact, to obtain a reliable empirical resistivity-salinity relationship, the ERT images must have a high resolution [32] and for this the depth of investigation must not exceed 5 m below the ground. This leads to a short inter-electrode spacing and to the high resolution ERT images.

A rock electrical resistivity value in the upper part of the aquifer at a depth of 1 m below the water table close was derived from each ERT carried out close the borehole. The measurements were correlated with the salt concentration measured at the same depth in the water of boreholes. Thus, groundwater salt concentration (g/L) as a function of the soil resistivity [33] was estimated by using

$$C_{salt} = a\rho^b \tag{7}$$

where a (= 47.02) and b (= -0.7) are two dimensionless best fit (R^2 = 0.93) constants and ρ (Ωm) is the monitored electrical resistivity of the groundwater. Despite of the few (six) boreholes considered, the spread of measured values of water salinity, which ranged from 1 to 5 g/L, allowed a high (Figure 4) correlation coefficient. The graph shows a lack of information for salt concentrations higher than 5 g/L, due to the absence of boreholes.

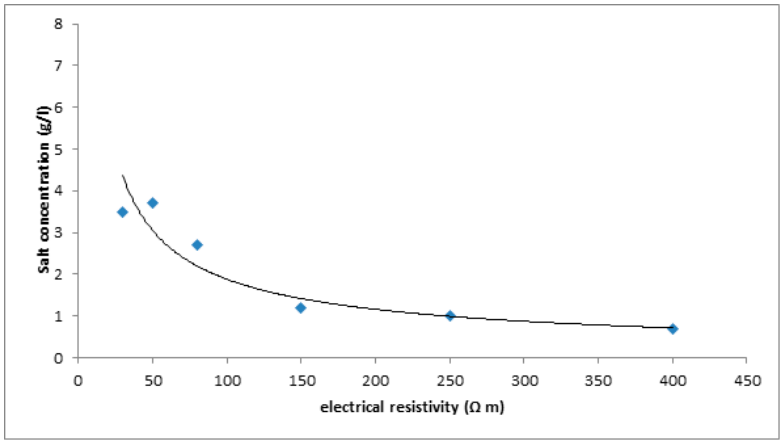

Figure 4. The relationship between electrical resistivity (ρ) and groundwater salt concentration (C_{salt}) at the Bari coastal aquifer.

3. Results and Discussion

Flow model results (Figure 5) provide freshwater heads (m) and freshwater velocity and discharge in each grid channel of discretized aquifer domain of 7200 × 6300 m^2.

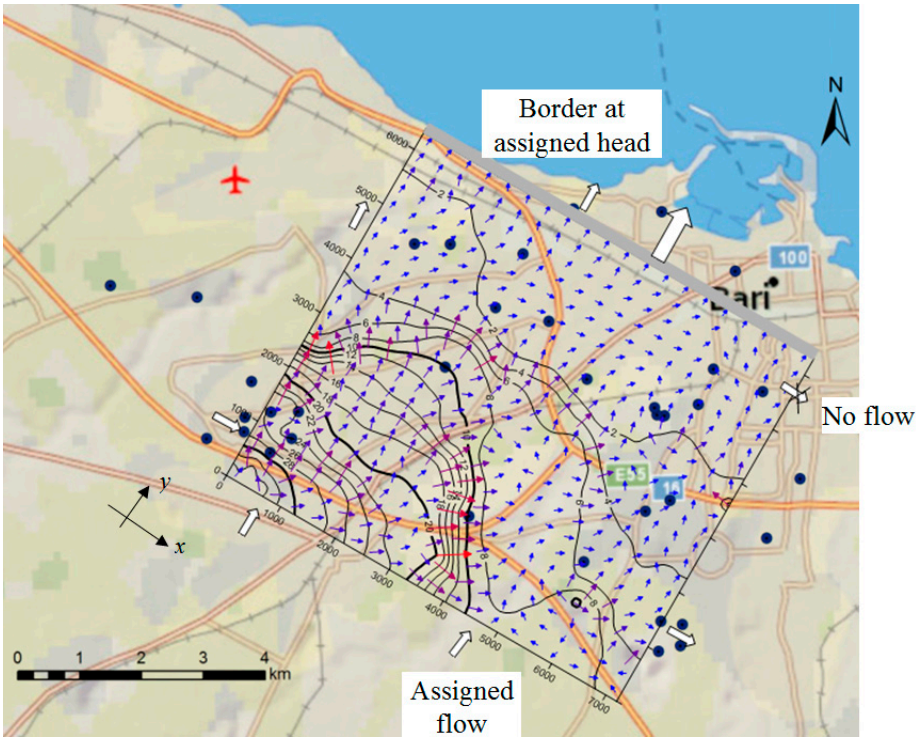

Figure 5. Model output: Freshwater heads (contour lines) in meters above sea level and water velocities (vectors) ranging from 10 (in blue) to 80 m/d (in red) in the studied area. White arrows and the gray border indicate the boundary conditions imposed during flow simulations; solid circles are wells.

Each horizontal fracture, at the regional scale, belonging to the 3D parallel set was discretized using a grid step size of $\Delta x = \Delta y = 150$ m (i.e., 49 × 43 grid nodes). The saturated aquifer thickness was 30 m, on average, and by considering an average aperture of 0.47 mm for each single fracture of the set, a total of 80 fractures were estimated for an effective porosity of 0.35% [23]. The conceptual fractured model used in this work was derived from the layered model [24] and is made up of several horizontal fractures bounded by impermeable rocks [25]. This is because vertical or sub vertical fractures that usually occur in these limestone formations, which are formed by the movements of tectonic plates, are very infrequent, so groundwater does not generally flow, as in the vertical lattice of fractures. This means that, although vertical connections between horizontal (and parallel) fractures of the coastal aquifer exist, horizontal preferential pathways dominate the water flow and each vertical fracture acts like a piezometer of an aqueduct comprising parallel pipelines: it ensures that the freshwater flows in each sub horizontal (and parallel) fracture (or pipe) with the same head gradient line. The freshwater discharge in each grid channel allows the estimation of the sharp interface position in the coastal area. For this calculation, an Excel (Microsoft) sheet was implemented with Equation (5) in order to estimate the $L - L_d$ distance for each Δx along the coast. Then, the coast distance y_d from the border domain at the assigned head (see Figure 5) was also considered to estimate all L_d distances with respect to the coastline. Finally, the application of Equation (6) to all grid nodes of the domain led to a salinity map of the Bari aquifer (Figure 6), at a depth of 1 m below the water table.

Figure 7 shows the results of the inverted ERT profiles at Line A and Line B. A common colour scale has been settled in order to point out the differences in electrical resistivity between Line A

(Figure 7a) and Line B (Figure 7b) profiles. Due to the great size of the studied area with respect to the length of the geophysical profiles, the ERT images are shown unscaled.

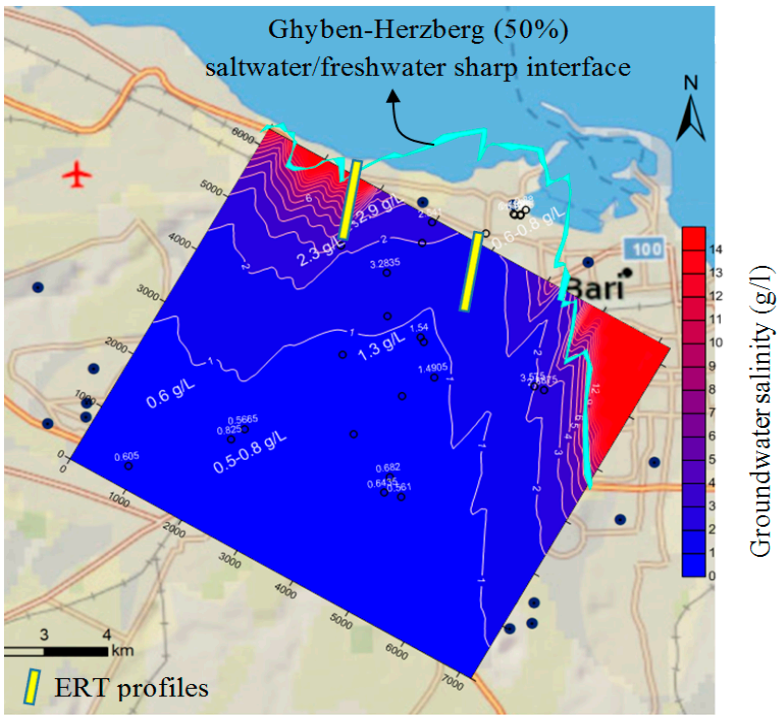

Figure 6. Groundwater salinity map (at a depth of 1.0 m below the water table) given by Ghyben-Herzberg and flow simulation results at the Bari coastal aquifer. Open circles are measured salinities in boreholes.

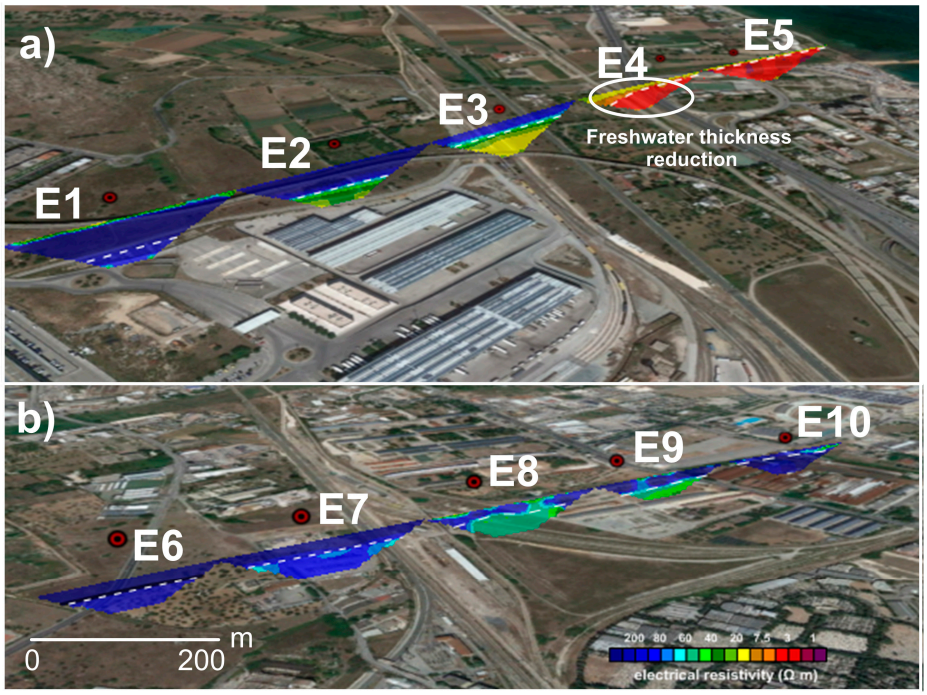

Figure 7. Inverted ERT profiles at Line A (**a**) (from E1 to E5) and at Line B (**b**) (from E6 to E10): ERT model error: <5%. E4 shows freshwater thickness reduction due to seawater intrusion.

Vertical and horizontal exaggerations in Figure 7 highlighted the change of electrical resistivity of monitored groundwater along each profile section. White dashed line shows the position of the water table at a depth of 1.5–15 m below the ground given by the flow model and the field measurements. From upstream to downstream, Line A highlights a significant decrease of aquifer resistivity, from values higher than 200–300 Ωm to values less than 5 Ωm. In particular, low resistivity values in E4–E5 (on the Line A) (see Figure 7a) show a decrease of freshwater thickness associated to the inland seawater intrusion. On the contrary, only a small range of resistivity from the high values of 200–300 Ωm associated with freshwater to the values of 40–60 Ωm, was recorded along the Line B. This is because fractures along Line B transport high freshwater water flows due to the large size of the fracture apertures, by avoiding seawater intrusion. These geophysical results agree with the model outputs, confirming ERT is a valuable technique to detect the seawater intrusion in groundwater. In order to provide a quantitative estimation of the salt concentration in groundwater a new relationship ρ-C_{salt} was implemented to convert the collected electrical resistivity into salt concentrations in groundwater. In order to compare the groundwater salinity derived from ERT profiles with modeling results, the two trends of salinities estimated by ERT into the Bari coastal aquifer have been plotted in Figure 8, together with results derived from model flow simulations (by including Ghyben-Herzberg estimations) at the depth of 1 m below the water table. This result successful validated the modeling output and at same time shows the efficacy of ERT to prove, experimentally, the seawater encroachment along the coast. Moreover direct measurements in boreholes by probes can be affected by the mixing due to water inflow coming from fractures at different depths of the water column, whereas the salinity estimations derived from ERT measurements can better represent real salt concentration into the fractures at a specific depth. This can be a valid support for modeling validations.

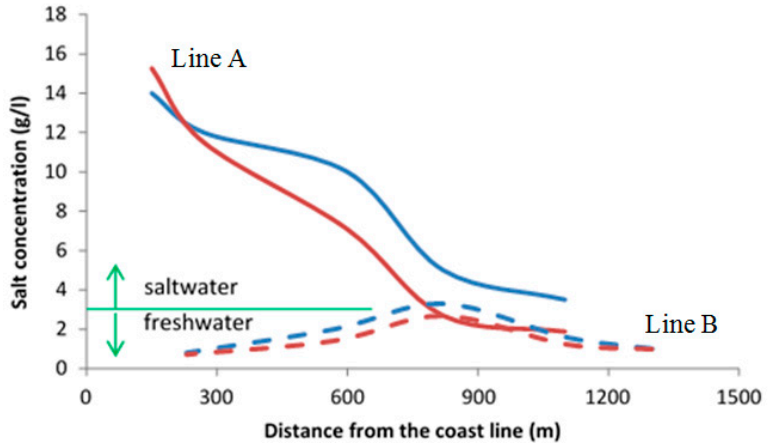

Figure 8. Comparison between salinity trends estimated by using ERT (red lines) and by using the Ghyben Herzberg model (blue lines). Solid lines represent the Line A groundwater section; dotted lines represent the Line B groundwater section.

4. Conclusions

The proposed case study deals with an innovative approach to model flow and salt transport phenomena in fractured coastal aquifers affected by seawater intrusion. The adopted procedure is based on a stochastic method able to transfer all real filtration medium heterogeneities into the numerical flow model. In particular, the stochastic method applied in this work investigated the spatial variability related to the size of the fracture apertures of the Bari groundwater. The model implemented the Ghyben-Herzberg to estimate groundwater salinity by means of sharp freshwater/saltwater position along the coast. The result provided the map of groundwater salinity at the depth of 1 m below water table, visualising the sea encroachment in groundwater and the freshwater flow in different areas along the coast. The main advantage of the proposed approach lies in the capability of

the model to simulate flow and salt transport processes in complex hydrogeological systems, where the wide heterogeneous nature of the fractured rock and the small size of the fracture aperture make difficult the application of the conventional flow equation, such as Darcy's law to a groundwater representative volume. However, at the field scale, it should also be considered the uncertainty (about 15%) due to prediction of spatial covariance of fracture apertures, which is dependent upon the available number of field measurements (i.e., well pumping-tests). For this, the ERT technique has proven to be a useful tool for the validation and uncertainty reduction of the flow and transport numerical model in fractured coastal aquifers affected by seawater intrusion. Moreover, ERT derived salt concentration data may overcome the issue related to the mixing of the fracture fluxes that occur inside the borehole at different depths of the water columns. Hence, ERT may give more reliable salt concentration values in comparison with measurements carried out in boreholes without using packers. However in order to improve numerical model solutions and the accuracy of petro-physical relationship ρ-C_{salt}, a higher number (>40) of appropriate measurements in wells is required.

Author Contributions: Costantino Masciopinto developed the mathematical model, collected field pumping tests and salinity measurements, and carried out model simulations. Lorenzo De Carlo and Maria Clementina Caputo conceived and designed the experimental geophysical tests; and Lorenzo De Carlo and Isabella Serena Liso performed the geophysical survey and analyzed the data. Each author has contributed to the writing of the manuscript.

Conflicts of Interest: The authors declare no conflict of interest.

References

1. Diersch, H.J. *FEFLOW: Finite Element Modeling of Flow, Mass and Heat Transport in Porous and Fractured Media*; Springer: Heidelberg, Germany, 2009; ISBN 978-3-642-38739-5.
2. Voss, C.I. *A Finite-Element Simulation Model for Saturated-Unsaturated, Fluid-Density-Dependent Groundwater Flow with Energy Transport or Chemically-Reactive Single-Species Solute Transport: U.S. Geological Survey Water-Resources Investigations Report*; US Geological Survey: Reston, VA, USA, 2009; Volume 84, p. 4369. Available online: https://pubs.usgs.gov/wri/1984/4369/report.pdf (accessed on 8 November 2017).
3. Simpson, M.J. Software Spotlight/SEAWAT-2000: Variable-Density Flow Processes and Integrated MT3DMS Transport Processes. *Ground Water* **2004**, *42*, 642–645. [CrossRef]
4. Werner, A.D.; Bakker, M.; Post, V.E.A.; Vandenbohede, A.; Lu, C.; Ataie-Ashtiani, B.; Simmons, C.; Barry, D.A. Seawater intrusion processes, investigation and management: Recent advances and future challenges. *Adv. Water Resour.* **2013**, *51*, 3–26. [CrossRef]
5. Masciopinto, C.; Palmiotta, D. Flow and Transport in Fractured Aquifers: New Conceptual Models Based on Field Measurements. *Transp. Porous Media* **2012**, *96*, 117–133. [CrossRef]
6. Tsang, Y.W.; Tsang, C.F.; Hale, F.V.; Dverstorp, B. Tracer transport in a stochastic continuum model of fractured media. *Water Resour. Res.* **1996**, *32*, 3077–3092. [CrossRef]
7. Schwartz, F.; Smith, L.; Crowe, A. A stochastic analysis of macroscopic dispersion in fractured media. *Water Resour. Res.* **1983**, *19*, 1253–1265. [CrossRef]
8. Chiles, J.P.; De Marsily, G. Stochastic Models of Fracture System and Their Use in Flow and Transport Modeling. In *Flow and Contaminant Transport in Fractured Rock*; Bear, J., Tsang, C.F., De Marsily, G., Eds.; Academic Press: San Diego, CA, USA, 1993; pp. 169–236.
9. Nordqvist, W.A.; Tsang, Y.W.; Tsang, C.F.; Dverstorp, B.; Andersson, J. Effects of high variance of fracture transmissivity on transport and sorption at different scales in a discrete model for fractured rocks. *J. Contam. Hydrol.* **1996**, *22*, 39–66. [CrossRef]
10. Kazemi, H.; Gilman, J.R. Multiphase flow in fractured petroleum reservoirs. In *Flow and Contaminant Transport in Fractured Rock*; Bear, J., Tsang, C.-F., De Marsily, G., Eds.; Academic Press, Inc.: London, UK, 1993; Volumes 6–19, pp. 270–272.
11. Gelhar, L.W. *Stochastic Subsurface Hydrology*; Prentice-Hall, Inc.: Englewood Cliffs, NJ, USA, 1993; pp. 230–234, ISBN 978-0138467678.
12. Carter, A.R.J. Investigation into the Use of Resistivity Profiling in the Detection of the Fresh/Saline Water Interface within Coastal Settings. Bachelor's Thesis, University of Lancaster, Lancaster, UK, 2002; p. 71.

13. Cassiani, G.; Bruno, V.; Villa, A.; Fusi, N.; Binley, A.M. A saline trace test monitored via time-lapse surface electrical resistivity tomography. *J. Appl. Geophys.* **2006**, *59*, 244–259. [CrossRef]
14. Choudhury, K.; Saha, D.K. Integrated geophysical and chemical study of saline water intrusion. *Ground Water* **2004**, *42*, 671–677. [CrossRef] [PubMed]
15. Cimino, A.; Cosentino, C.; Oieni, A.; Tranchina, L. A geophysical and geochemical approach for seawater intrusion assessment in the Acquedolci coastal aquifer (Northern Sicily). *Environ. Geol.* **2008**, *55*, 1473–1482. [CrossRef]
16. De Franco, R.; Biella, G.; Tosi, L.; Teatini, P.; Lozej, A.; Chiozzotto, B.; Giada, M.; Rizzetto, F.; Claude, C.; Mayer, A.; et al. Monitoring the saltwater intrusion by time lapse electrical resistivity tomography: The Chioggia test site (Venice Lagoon, Italy). *J. Appl. Geophys.* **2009**, *69*, 117–130. [CrossRef]
17. Gnanasundar, D.; Elango, L. Groundwater quality assessment of a coastal aquifer using geoelectrical techniques. *Int. J. Environ. Hydrol.* **1999**, *7*, 21–33.
18. Nowroozi, A.A.; Horrocks, S.B.; Henderson, P. Saltwater intrusion into the freshwater aquifer in the eastern shore of Virginia: A reconnaissance electrical resistivity survey. *J. Appl. Geophys.* **1999**, *42*, 1–22. [CrossRef]
19. Sathish, S.; Elango, L.; Rajesh, R.; Sarma, V.S. Assessment of seawater mixing in a coastal aquifer by high resolution electrical resistivity tomography. *Int. J. Environ. Sci. Tech.* **2009**, *8*, 483–492. [CrossRef]
20. Shammas, M.I.; Jacks, G. Seawater intrusion in the Salalah plain aquifer. *Oman. Environ. Geol.* **2007**, *53*, 575–587. [CrossRef]
21. Urish, D.W.; Frohlich, R.K. Surface electrical resistivity in coastal groundwater exploration. *Geoexploration* **1990**, *26*, 267–289. [CrossRef]
22. Wagner, F.M.; Möller, M.; Schmidt-Hattenberger, C.; Kempka, T.; Maurer, H. Monitoring freshwater salinization in analog transport models by time-lapse electrical resistivity tomography. *J. Appl. Geophys.* **2013**, *89*, 84–95. [CrossRef]
23. Singha, K.; Gorelick, S.M. Saline tracer visualized with three-dimensional electrical resistivity tomography: Field-scale spatial moment analysis. *Water Resour. Res.* **2005**, 41. [CrossRef]
24. Archie, G.E. The electrical resistivity log as an aid in determining some reservoir characteristics. *Trans. Am. Inst. Min. Metall. Pet. Eng.* **1942**, *146*, 54–62. [CrossRef]
25. Masciale, R.; De Carlo, L.; Caputo, M.C. Impact of a very low enthalpy plant on a costal aquifer: A case study in Southern Italy. *Environ. Earth Sci.* **2015**, *74*, 2093–2144. [CrossRef]
26. Pieri, P.; Sabato, L.; Spalluto, L.; Tropeano, M. Note illustrative della carta geologica dell'area urbana di Bari in scala 1:25.000 (notes of the geological map of the urban area of Bari at scale 1:25.000). *Rend. Online Soc. Geol. Ital.* **2011**, *14*, 26–36. [CrossRef]
27. Masciopinto, C.; La Mantia, R.; Chrysikopoulos, C.V. Fate and transport of pathogens in a fractured aquifer in the Salento area, Italy. *Water Resour. Res.* **2008**, *44*, 1–18. [CrossRef]
28. Bear, J. *Dynamics of Fluids in Porous Media*; American Elsevier Publishing Company, Inc.: New York, NY, USA, 1972; pp. 25–170.
29. Fiori, A.; Bellin, A. Non-ergodic transport of kinetically sorbing solutes. *J. Contam.* **1999**, *40*, 201–219. [CrossRef]
30. Masciopinto, C.; Liso, I.S. Assessment of the impact of sea-level rise due to climate change on coastal groundwater discharge. *Sci. Total Environ.* **2016**, *569*, 672–680. [CrossRef] [PubMed]
31. Masciopinto, C.; Palmiotta, D. A New Method to Infer Advancement of Saline Front in Coastal Groundwater Systems by 3D: The Case of Bari (Southern Italy) Fractured Aquifer. *Computation* **2016**, *4*, 9. [CrossRef]
32. Binley, A.; Kemna, A. DC Resistivity and Induced Polarization Methods. In *Hydrogeophysics*; Rubin, Y., Hubbard, S.S., Eds.; Springer: Dordrecht, The Netherlands, 2005; pp. 129–156, ISBN 101-4020-3101-7.
33. Keller, G.V.; Frischknecht, F.C. Electrical Methods in Geophysical Prospecting, Pergamon, London. 1996. Available online: https://www.eoas.ubc.ca/ubcgif/iag/foundations/properties/resistivity.htm (accessed on 11 September 2017).